

MIT Open Access Articles

Evaluation and Analysis of Next-Generation FY-4A LPW Products over Various Climatic Regions in China

The MIT Faculty has made this article openly available. **Please share** how this access benefits you. Your story matters.

Citation: Zhang, W.; Xiao, X.; Peng, J.; Zhang, S.; Shehaj, E.; Moeller, G. Evaluation and Analysis of Next-Generation FY-4A LPW Products over Various Climatic Regions in China. *Atmosphere* 2024, 15, 1545.

As Published: <http://dx.doi.org/10.3390/atmos15121545>

Publisher: Multidisciplinary Digital Publishing Institute

Persistent URL: <https://hdl.handle.net/1721.1/157961>




Version: Final published version: final published article, as it appeared in a journal, conference proceedings, or other formally published context

Terms of use: Creative Commons Attribution



Article

Evaluation and Analysis of Next-Generation FY-4A LPW Products over Various Climatic Regions in China

Wenyuan Zhang ^{1,2,*} , Xinyu Xiao ¹, Jinsong Peng ¹, Shubi Zhang ^{1,*}, Endrit Shehaj ^{2,3}  and Gregor Moeller ⁴ 

¹ School of Environment and Spatial Informatics, China University of Mining and Technology, Xuzhou 221116, China; ts24160044a31@cumt.edu.cn (X.X.); ts24160187p31@cumt.edu.cn (J.P.)

² Institute of Geodesy and Photogrammetry, ETH Zurich, 8093 Zurich, Switzerland; eshehaj@mit.edu

³ Department of Aeronautics and Astronautics, Massachusetts Institute of Technology, Boston, MA 02139, USA

⁴ Department of Geodesy and Geoinformation, TU Wien, 1040 Vienna, Austria; gregor.moeller@geo.tuwien.ac.at

* Correspondence: zhangwy@cumt.edu.cn (W.Z.); zhangshubi@cumt.edu.cn (S.Z.)

Abstract: Atmospheric water vapor, a significant constituent of the atmosphere, affects the energy balance between Earth's atmosphere and space, and its changes play a crucial role in the greenhouse effect. Layer precipitable water (LPW), which represents the column-integral water vapor within a vertical range, is increasingly recognized as a key indicator of atmospheric water vapor distributions and variations. Due to its capability for layer-wise monitoring, LPW products have the potential to offer valuable insights into the characteristics and evolution of climatic regions through refined atmospheric spatiotemporal information. However, the observational quality and spatiotemporal variations of LPW products across different climate zones, e.g., the diverse climatic regions in China, have not been systematically assessed. In this paper, we aim to evaluate and analyze the climatic and seasonal variations of FY-4A LPW products across five climatic regions in China, contributing to a deeper understanding of water vapor variability and providing valuable data for climate change research. A surface pressure calibration algorithm for ERA5 data is developed to calculate accurate ERA5 LPW products. The results show that all four FY-4A LPWs are consistent with ERA5 LPWs, with an overall root mean square error (RMSE) of 2.58, 0.90, 1.30, and 1.01 mm, respectively. Furthermore, FY-4A LPWs are underestimated in the temperate monsoon area and overestimated in the subtropical and tropical monsoon regions, while FY-4A observations agree well with ERA5 reanalysis in temperate continental and plateau mountain zones. These analyses highlight the remarkable climate dependency of FY-4A LPWs and their potential for climate-related studies.

Keywords: layer precipitable water (LPW); Fengyun-4A; ERA5; quality evaluation; variation analysis



Citation: Zhang, W.; Xiao, X.; Peng, J.; Zhang, S.; Shehaj, E.; Moeller, G. Evaluation and Analysis of Next-Generation FY-4A LPW Products over Various Climatic Regions in China. *Atmosphere* **2024**, *15*, 1545. <https://doi.org/10.3390/atmos15121545>

Academic Editors: Fei Yang, Ming Shangguan, Liangke Huang, Di Zhang and Filomena Romano

Received: 30 October 2024

Revised: 1 December 2024

Accepted: 12 December 2024

Published: 23 December 2024



Copyright: © 2024 by the authors. Licensee MDPI, Basel, Switzerland. This article is an open access article distributed under the terms and conditions of the Creative Commons Attribution (CC BY) license (<https://creativecommons.org/licenses/by/4.0/>).

1. Introduction

Water vapor, one of the vital elements of the atmosphere, plays an essential role in climate change, extreme weather evolution, global water cycle, and energy balance [1–5]. Presently, various meteorological parameters related to water vapor have been defined to represent the state of atmospheric water vapor, e.g., partial pressure of water vapor, water vapor density, water vapor mixing ratio, specific humidity, relative humidity, integrated water vapor (IWV), and precipitable water vapor (PWV) [6,7]. PWV, the most commonly used and crucial indicator, represents the total atmospheric water vapor along a vertical column [8]. It has been successfully applied to reconstruct high resolution water vapor maps, forecast extreme rainfalls, and investigate the climate change [9–12]. Compared to PWV, layer precipitable water (LPW) reports the column-integral water vapor content within a specified vertical range, showing significant potential for monitoring the layer-wise level moisture advection and variation [13]. Thus, Wang et al. assimilate the LPW products into a numerical weather prediction (NWP) model to improve local

severe storm forecasts [14]. In addition, the impact of LPW and cloud water path data on short-term convective-scale NWP forecasts has also been examined [15].

The sensors installed on geostationary orbit (GEO) meteorological satellites are the main and significant instruments for sensing LPW products with large regional or global scales [16]. Currently, the next-generation GEO meteorological satellites are developing vigorously, e.g., FenYun-4 (FY-4) from China, Geostationary Operational Environmental Satellite-R (GOES-R) from America, and Himawari-8/-9 from Japan [13,14,17]. FY-4A is the first satellite of the FY-4 series that represents the Chinese new generation geostationary meteorological satellites. It carries four instruments: the advanced geosynchronous radiation imager (AGRI), the geostationary interferometric infrared sounder (GIIRS), the lightning mapping imager (LMI), and the space environment package (SEP), with the main objectives of monitoring the rapid weather change and improving severe weather forecasting [17]. FY-4A observations yield a number of new meteorological and environmental products over China and adjacent regions, which contribute to improving the understanding and forecasting of China's climate, environment, and disasters. AGRI, one of the key instruments installed on the FY-4A satellite, is characterized by the high accuracy, fast scanning, and high efficiency. It is able to retrieve four LPW products: total perceptible water (TPW), low layer perceptible water (PW_low), middle layer perceptible water (PW_mid), and high layer perceptible water (PW_high) [17].

The above next-generation LPW products are beneficial for monitoring the convection in the atmosphere and analyzing the variation trend of water vapor at different altitudes. It is necessary to evaluate the reliability and applicability of AGRI LPW retrievals over China to maximize the significance of LPW products for meteorological research. Moreover, the East Asian monsoon and the large topographic changes result in the various climate types with dramatic differences, which thus causes the water vapor distributions in China to show significant climatic and seasonal changes [18]. Therefore, it is urgent to adequately analyze the distribution and variety of next-generation LPW products over different climatic regions during different seasons.

In this study, we aim to evaluate and analyze the climatic and seasonal variations of FY-4A LPW products across five climatic regions in China. It is hypothesized that variations in water vapor content across different climatic regions may offer valuable insights into climate patterns and enhance our understanding of regional climatic differences. The fifth generation European Centre for Medium-Range Weather Forecasts (ECMWF) atmospheric reanalysis data (ERA5) are utilized as reference data. This choice is based on its notable advantages of long-term continuity and high, uniform spatiotemporal resolution compared to other measurements. In addition, the feasibility of using PWV products obtained from the latest ERA5 atmospheric reanalysis for climate change analysis has been fully validated [19]. Regarding the limitations, since the main goal of this study is the evaluation and analysis of FY-4A LPW products, we did not investigate the underlying drivers of the observed variations in water vapor. We recognize the significance of such an analysis and plan to explore the relationship between LPW variations and climate change in future research.

This article is organized as follows: In Section 2, we report on the datasets and LPW calculation methods and introduce a surface pressure calibration algorithm for the ERA5 data. Section 3 evaluates the overall performance of FY-4A LPW products and analyzes its temporal and spatial variation trends over multiple climatic regions in China. The comprehensive analysis of FY-4A LPW products during five climatic regions are performed in Section 4. Section 5 discusses the comparisons of FY-4A LPW products in different climatic areas and seasons, respectively. Finally, the conclusions are drawn in Section 6.

2. Data and Methods

2.1. FY-4A and ERA5 Data

In this study, four types of LPW products obtained from AGRI are employed for the evaluations, i.e., TPW, PW_low, PW_mid, and PW_high. AGRI has three operation modes: full disk area every 15 min, China area every 5 min, and target area every 1 min [20]. The

AGRI LPW products are openly accessible and can be freely downloaded from the Fengyun Satellite Data Center (available at <https://satellite.nsmc.org.cn/portalsite/default.aspx?currentculture=en-US> (accessed on 1 February 2024)).

To validate the performance of FY-4A LPW retrievals over different climatic types in China, the LPW data with 5 min resolution over China area for the whole year 2020 are used. Commonly, China is divided into five climate zones: temperate monsoon, temperate continental, plateau mountain, subtropical monsoon, and tropical monsoon climatic areas. Their climate characteristics are as follows: (1) the temperate monsoon zone, characterized by hot, humid summers and cold, dry winters; (2) the temperate continental zone, with hot summers, cold winters, and low precipitation; (3) the plateau mountain zone, marked by cool temperatures year-round, with mild summers and cold winters at higher altitudes; (4) the subtropical monsoon zone, which experiences hot, humid summers and mild, wet winters with abundant rainfall; and (5) the tropical monsoon zone, located in southern China, with warm temperatures year-round and significant rainfall during the summer monsoon season [21–23].

As for the division criteria of these climatic zones, we use the precise climate zone classification from the Atlas of Climate of the P.R. of China [24], which is widely used as a reference in climate-related studies in the China region [25]. Figure 1 illustrates the distribution of these five climatic zones across China. The FY-4A LPW products are retrieved from the atmospheric layer integrated moisture of AGRI field of views (FOVs) using the physical retrieval algorithm described by [17], with the spatial resolution of 4 km.

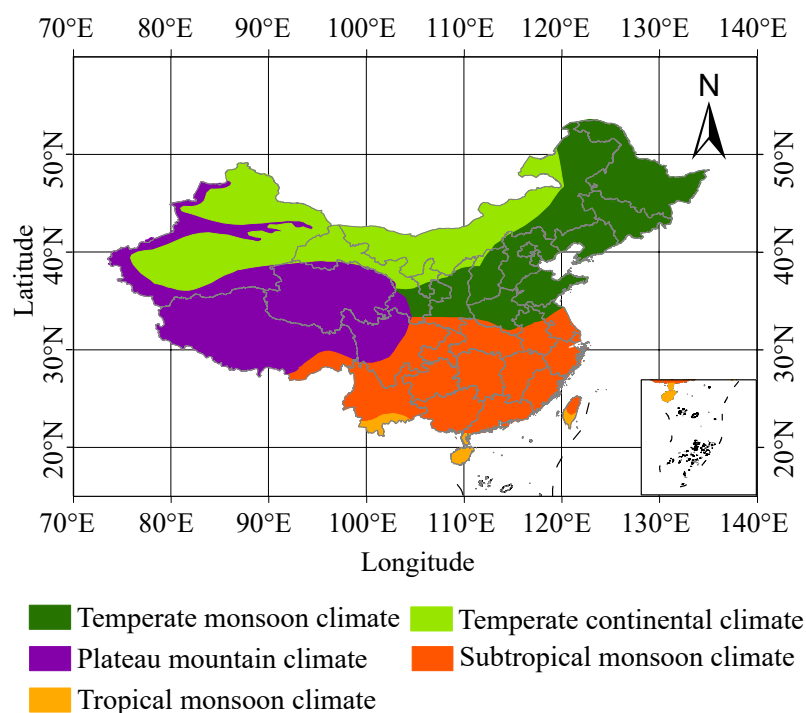


Figure 1. Geographic distribution of the five climatic regions over China.

As for the ERA5 data, they are in the state-of-the-art ECMWF global reanalysis dataset, which can be freely downloaded from the Copernicus Climate Data Store [26]. Compared to the predecessor ERA-Interim data (third-generation global atmospheric reanalysis), ERA5 has a higher spatial and temporal resolution capability (0.25°/1-h vs. 0.75°/6-h) and a more advanced data assimilation system, implying the great potential to monitor and analyze the atmospheric water vapor using the high spatiotemporal ERA5-derived products.

In this study, we use the ERA5 hourly data on pressure levels from 1940 to the present (available at <https://cds.climate.copernicus.eu/datasets/reanalysis-era5-pressure-levels?tab=download> accessed on 1 February 2024). These data were accessed in March 2024. In

China, the ERA5-derived PWV error is generally less than 1 mm when comparing with the PWV products from the Chinese ground meteorological stations, which indicates that ERA5 can support high-accuracy PWV evaluations and calibrations over China [27]. The hourly meteorological parameters (e.g., temperature, specific humidity, relative humidity) and geopotential on 37 pressure levels from ERA5 pressure level products at full resolution (0.25°) are adopted for the evaluations and analyses of the FY-4A LPW data in this paper.

2.2. Physical Algorithm for Retrieving FY-4A LPW Products

In the AGRI physical retrieval algorithm, due to the rare water vapor above 300 hPa, only water vapor contents from surface to 300 hPa are considered for the retrieval of LPW products. Therefore, TPW is defined as the amount of water vapor in the column of the unit cross-section area within this range. The other three LPWs correspond to the three pressure ranges of surface to 900 hPa, 900 to 700 hPa, and 700 to 300 hPa [17]. However, in some areas, the surface pressure could be lower than 900 hPa, even less than 700 hPa in the high altitude regions. To solve this case, a sigma pressure ordinate is adopted in AGRI observations. In the sigma pressure ordinate, the boundary pressures for the retrieval of LPWs, i.e., the surface pressure, 900 hPa, 700 hPa, and 300 hPa, are converted into the sigma indexes of 1.0, 0.9, 0.7, and 0.3, respectively. The conversion formula of sigma pressure ordinate is as follows [13,14,28]:

$$P_{\sigma} = 0.005 + \sigma \cdot (P_{sur} - 0.005) \quad (1)$$

where P_{σ} denotes the sigma pressure corresponding to the sigma index value of σ , and P_{sur} represents the local surface pressure. For example, when the surface pressure is less than 1000 hPa, such as 850 hPa, we substitute the surface pressure $P_{sur} = 850$ hPa into (1) and obtain $P_{\sigma=0.9} = 765.0005$ hPa, $P_{\sigma=0.7} = 595.0015$ hPa, and $P_{\sigma=0.3} = 255.0035$ hPa.

A linear interpolation along the vertical pressure direction is employed to determine the water vapor mixing ratio q at the special levels, as shown in the following equation [16]:

$$q(P_{\sigma}) = q(P_{below}) + [q(P_{above}) - q(P_{below})] \cdot \left[\frac{\ln q(P_{\sigma}) - \ln q(P_{below})}{\ln q(P_{above}) - \ln q(P_{below})} \right] \quad (2)$$

where $q(P_{\sigma})$ is the water vapor mixing ratio value at P_{σ} level. $q(P_{above})$ and $q(P_{below})$ represent the water vapor mixing ratio at P_{above} and P_{below} levels, respectively, corresponding to the upper and lower levels immediately adjacent to the P_{σ} level. With the pressure and moisture profiles at sigma pressure levels, the LPWs can be calculated from the interpolated profiles using the below formula [13]:

$$LPW = \frac{10}{\rho_w g} \cdot \sum_{k=1}^n \frac{(q_k + q_{k+1}) \cdot (P_k - P_{k+1})}{2} \quad (3)$$

where ρ_w is the water density with a value of 1000 kg m^{-3} , g denotes the gravity acceleration. q_k and P_k represent the water vapor mixing ratio and pressure at k -th sigma pressure level, respectively. The four LPW retrievals then can be obtained with the above equation. For instance, when calculating the PW_mid, $P_{k=1}$ is the sigma pressure level of $P_{\sigma=0.9}$, while $P_{k=n}$ is the sigma level of $P_{\sigma=0.7}$.

2.3. Surface Pressure Calibration Algorithm for ERA5 LPW Products

ERA5 data is produced with 4D-Var data assimilation and model forecasts of the ECMWF Integrated Forecast System (IFS), providing atmospheric data at 37 pressure levels from standard 1000 to 1 hPa. Based on the geopotential, pressure and specific humidity profiles at these pressure levels, ERA5 LPW can be estimated [19]:

$$LPW = \frac{1}{g} \int_{P_a}^{P_b} q_v dP \quad (4)$$

where g is the same as in (3), P_a and P_b represent the pressure values, and q_v denotes the specific humidity.

It should be noted that the surface pressure in some regions is less than 1000 or 900 hPa, so the LPW calculation errors would be generated when the sigma pressure ordinate is directly imposed on the fixed ERA5 layer data, i.e., the data from 1000 to 300 hPa. To solve this issue, we need to use suitable reference elevation data to evaluate the ERA5 surface altitude. Given the global coverage, high spatial resolution, and precision of the TanDEM-X digital elevation model (DEM) products, we have used them as the reference data for this evaluation [29]. We develop a surface pressure calibration algorithm for ERA5 LPW products based on the high resolution DEM data. Figure 2 shows the flow chart of the surface pressure calibration algorithm, which includes several steps as below:

1. Transform the geopotential height value that is commonly adopted in ECMWF dataset into the elevation value following the procedures given in our previous studies [30,31].
2. Judge the difference between the ERA5 surface altitude and DEM value for each grid point. The threshold of difference is set to 10 m since the nominal accuracy of DEM data is 10 m [29], i.e., when the difference is larger than 10 m, the surface pressure of ERA5 data needs to be corrected.
3. Calculate the surface pressure based on the surface altitude from DEM using the exponential interpolation method:

$$P_s = \frac{h_s - h_{down}}{h_{up} - h_{down}} \cdot P_{down} \cdot e^{-\frac{h_s - h_{down}}{H_{scale}}} + \frac{h_{up} - h_s}{h_{up} - h_{down}} \cdot P_{up} \cdot e^{-\frac{h_s - h_{up}}{H_{scale}}} \quad (5)$$

where h_s is the surface altitude derived from DEM, P_s represents the pressure at DEM surface level. h_{up} and h_{down} denote the altitude values of ERA5 upper and lower levels adjacent to the h_s level. P_{up} and P_{down} are the corresponding pressures from the ERA5 data. H_{scale} represents the scale height and can be determined with ERA5 data [32].

4. Estimate the sigma pressure of ERA5 at four sigma indexes using (1). Subsequently, the specific humidity from the ERA5 data also is interpolated to the sigma pressures with (2). Furthermore, to improve the retrieval accuracy of ERA5 LPWs, we construct the dense ERA5 vertical layer observations with a 10 m interval using the exponential interpolation (5) and apply the Newton–Cotes formula to calculate the integration of (4) [32]:

$$LPW = \frac{1}{8} \sum_{k=1}^n \frac{\Delta P_k}{90} \cdot [7q_1^k + 32q_2^k + 12q_3^k + 32q_4^k + 7q_5^k] \quad (6)$$

where $q_1^k, q_2^k, q_3^k, q_4^k$, and q_5^k denote the specific humidity of the five interpolation points in the k -th level. ΔP represents the pressure interval of the k -th level.

To assess the performance of the developed algorithm, we use the radiosonde surface pressure data as a reference to evaluate the calibrated ERA5 surface pressure data. Due to their different temporal and spatial resolutions, the ERA5 grid data are matched to the radiosonde stations in time and space. Then, the ERA5-based surface pressure values at the radiosonde height are estimated using the developed algorithm. Figure 3 illustrates the RMSE of the ERA5 surface pressure at the matching radiosonde sites. It can be observed that the ERA5-based surface pressure data demonstrates high accuracy across all matching stations, with RMSE values generally below 1.5 hPa, and most values falling between 0 and 1 hPa. This confirms the strong performance of the surface pressure calibration algorithm and the reliability of the ERA5-based surface pressure data.

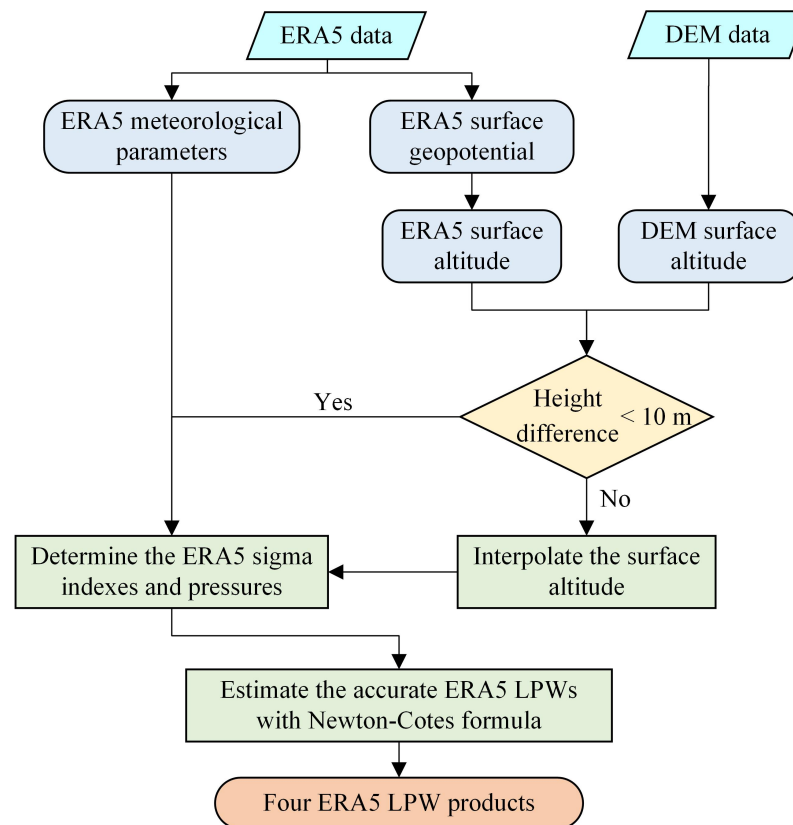


Figure 2. Flowchart illustration of surface pressure calibration algorithm for ERA5 LPW products.

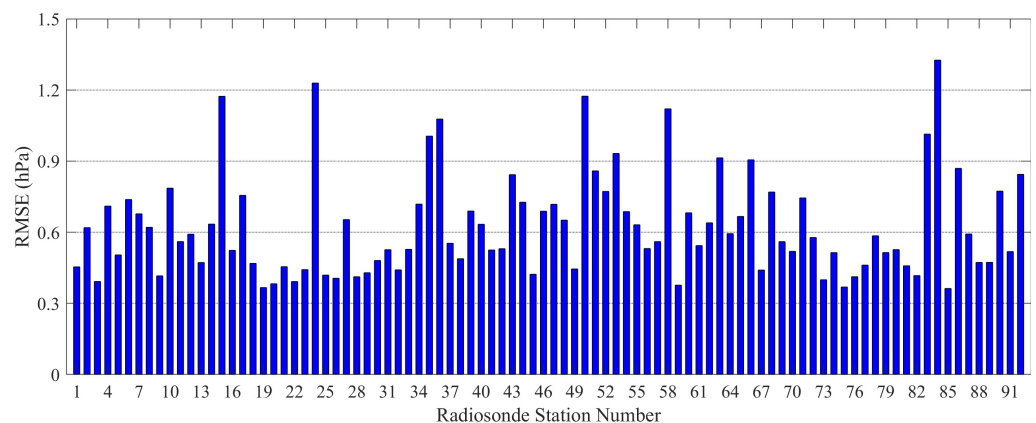


Figure 3. FLRMSE of the ERA5 surface pressure at the matching radiosonde sites in China.

2.4. Data Processing and Statistical Metrics

It should be noted that ERA5 only generates the water vapor products on the hour, while FY-4A LPWs show a higher time resolution of about 5 min with the China area scanning mode [20]. Therefore, the original FY-4A LPWs are sampled into hourly LPW products for the evaluation. In addition, as for the spatial matching scheme, the horizontal resolution of FY-4A LPWs is 4 km, while ERA5 data are gridded with a spatial resolution of 0.25° . Therefore, the inverse distance weighted (IDW) interpolation for FY-4A LPW products are performed to match the ERA5 grid points [33]. We selected IDW because it is a simple, widely used, and effective interpolation method that works well when there is a clear relationship between the distance and the variable being interpolated. This method is particularly suitable for matching the higher spatial resolution of FY-4A LPW data with the coarser resolution of ERA5 data.

To quantitatively evaluate and analyze the performance of FY-4A LPW products, three statistical metrics are utilized to assess the retrieval results, including root mean square error (RMSE), mean bias (MB), and correlation coefficient (R):

$$\text{RMSE} = \sqrt{\frac{\sum_{i=1}^n (\text{LPW}_{\text{ERA5}} - \text{LPW}_{\text{FY-4A}})^2}{n}} \quad (7)$$

$$\text{MB} = \frac{\sum_{i=1}^n (\text{LPW}_{\text{ERA5}} - \text{LPW}_{\text{FY-4A}})}{n} \quad (8)$$

$$\text{R} = \frac{\sum_{i=1}^n (\text{LPW}_{\text{ERA5}} - \overline{\text{LPW}}_{\text{ERA5}}) (\text{LPW}_{\text{FY-4A}} - \overline{\text{LPW}}_{\text{FY-4A}})}{\sqrt{\sum_{i=1}^n (\text{LPW}_{\text{ERA5}} - \overline{\text{LPW}}_{\text{ERA5}})^2 (\text{LPW}_{\text{FY-4A}} - \overline{\text{LPW}}_{\text{FY-4A}})^2}} \quad (9)$$

where LPW_{ERA5} and $\text{LPW}_{\text{FY-4A}}$ are the LPW observations provided by the ERA5 data and FY-4A AGRI infrared retrievals, respectively. $\overline{\text{LPW}}_{\text{ERA5}}$ and $\overline{\text{LPW}}_{\text{FY-4A}}$ correspond to the mean value of the two LPW products, and n denotes the number of LPW observations.

3. Evaluations and Variations of FY-4A LPW Products in China

The overall evaluations between FY-4A and ERA5 LPWs are illustrated in Figure 4, which indicates that all four FY-4A LPW products are generally consistent with the corresponding ERA5 LPWs. Each diagram contains more than 60 million data pairs. The four LPW products have the same number of pairs because they were extracted synchronously from the FY-4A satellite data. It is noticeable that TPW ranges from 0 to 80 mm, while PW_low varies between 0 and 20 mm, accounting for a quarter of the TPW. For PW_mid and PW_high, most observations of both products are less than 30 mm. As far as the accuracy of the four FY-4A LPW products is concerned, PW_low shows higher accuracy than the other three LPW products, with an RMSE of 0.90 mm, an MB of -0.09 mm, and an R of 0.97. On the contrary, the largest RMSE is generated by the FY-4A TPW product due to its large amounts, with a value of 2.58 mm. However, it shows the optimal R value (0.98). PW_mid and PW_high have comparable accuracy (1.30 mm vs. 1.01 mm in RMSE and 0.97 vs. 0.95 in R). Furthermore, the overall statistics of all FY-4A LPW products are calculated. The RMSE, MB, and R of FY-4A LPWs over China in 2020 are 1.43 mm, -0.05 mm, and 0.94, respectively, when compared with the ERA5 dataset.

To analyze the temporal variation characteristics of FY-4A LPW products, Figure 5a displays the monthly mean value of the four LPW products derived from FY-4A observations and ERA5 data from January to December 2020. TPW observations are approximately equal to the sum of the other three LPW products, so the four LPWs show the analogous variation trend that they gradually increase from January to April and then dramatically peak in July (with values of 23.64, 7.91, 10.45, and 5.37 mm for the four FY-4A LPWs), while they decrease continuously in the second half of 2020 (reaching minimums of 4.02, 1.47, 1.80, and 0.78 mm in December). As a whole, it is clear that the LPWs in summer (June to August) are significantly larger than those in other seasons. In addition, the monthly mean RMSE, MB, and R of FY-4A LPWs are shown in Figure 5b. It is noticeable that the RMSE displays the same seasonal pattern as LPW products, with the TPW RMSE varying between 1.57 mm in winter (December to February) and 3.86 mm in summer. The other three LPW RMSE values change between 0.56 mm and 1.90 mm with a similar tendency. In terms of MB, there is obvious overestimation for most FY-4A LPW products in most months, except PW_high values. The latter is overestimated in summer (MB = -0.09 mm) while underestimated in the other three seasons (0.14, 0.07, and 0.22 mm in MB) for AGRI observations. In R comparisons, the R values of TPW, PW_low, and PW_mid fluctuate between 0.94 and 0.98, revealing a good agreement with the three ERA5 LPWs, whereas the R of PW_high is unsatisfactory in some months, with a range from 0.89 to 0.96.

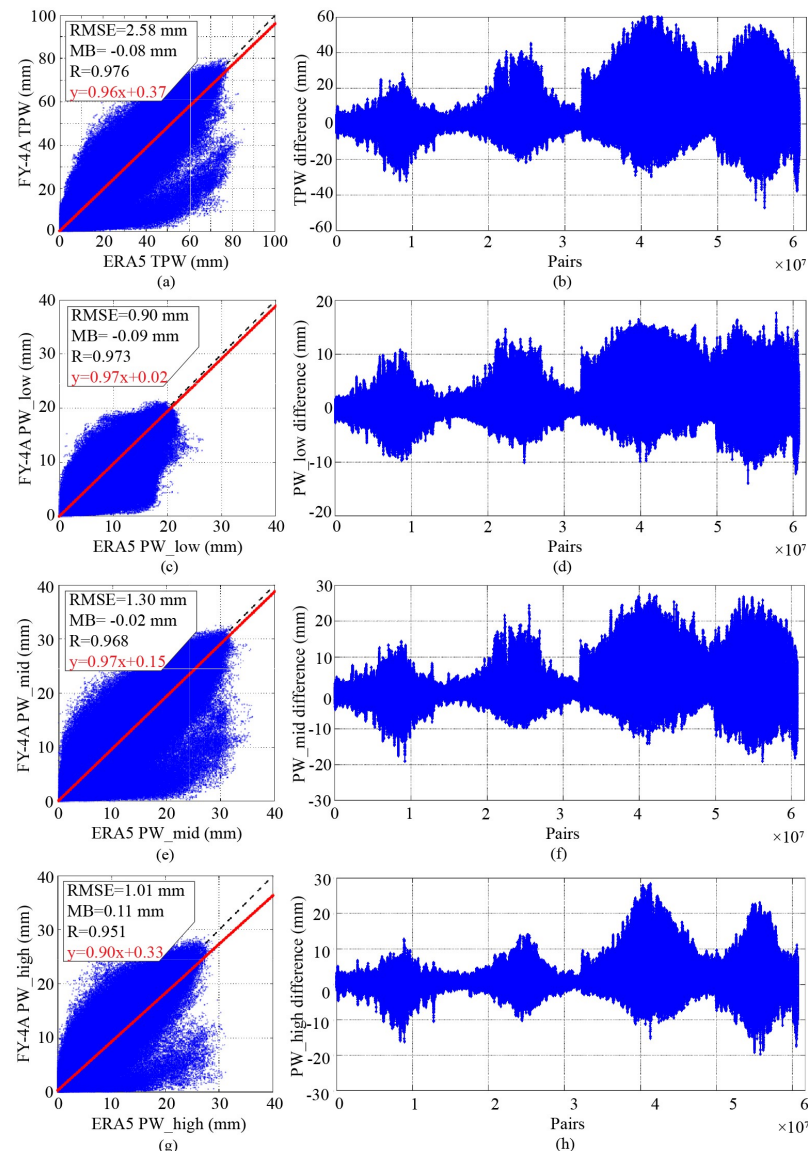


Figure 4. Scatterplots of FY-4A LPWs versus ERA5 LPW data and the distribution of the differences between the two observations (ERA5 minus FY-4A). (a) TPW product; (b) The difference for TPW; (c) PW_low product; (d) The difference for PW_low; (e) PW_mid product; (f) The difference for PW_L mid; (g) PW_high product; (h) The difference for PW_high; The dashed lines represent the zero-bias lines.

Furthermore, Figure 6 illustrates the spatial variations in LPWs from FY-4A and ERA5 in China, along with the difference obtained by ERA5 LPWs minus FY-4A LPWs. The results show that the spatial distribution of LPWs is remarkably related to the climate zones. For all four LPW products, both subtropical monsoon and tropical monsoon regions yield the largest LPW values, while the amount of LPWs in the plateau mountain area is the smallest. There are comparable LPW contents in temperate continental and temperate monsoon regions, except in the south of the latter. Meanwhile, the differences in four LPWs indicate the same spatial distributions, i.e., the larger differences in subtropical monsoon and tropical monsoon areas and the lower errors in plateau mountain region. This is mainly because the difference variations in LPWs are characterized by a significant dependence on the water vapor contents. Obviously, there are large water vapor disparities in different climatic areas. Meanwhile, the seasonal pattern also plays an important role in water vapor variations. Consequently, we need to deeply study their performance in different climatic regions from a seasonal perspective.

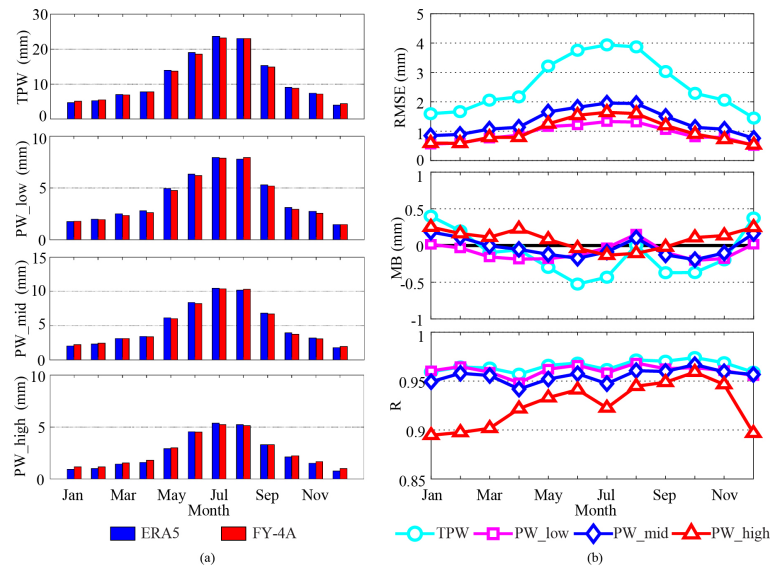


Figure 5. Monthly mean LPW comparison (a) obtained from FY-4A observations and ERA5 data and monthly mean statistics (b) of RMSE, MB, and R for the period from January to December 2020.

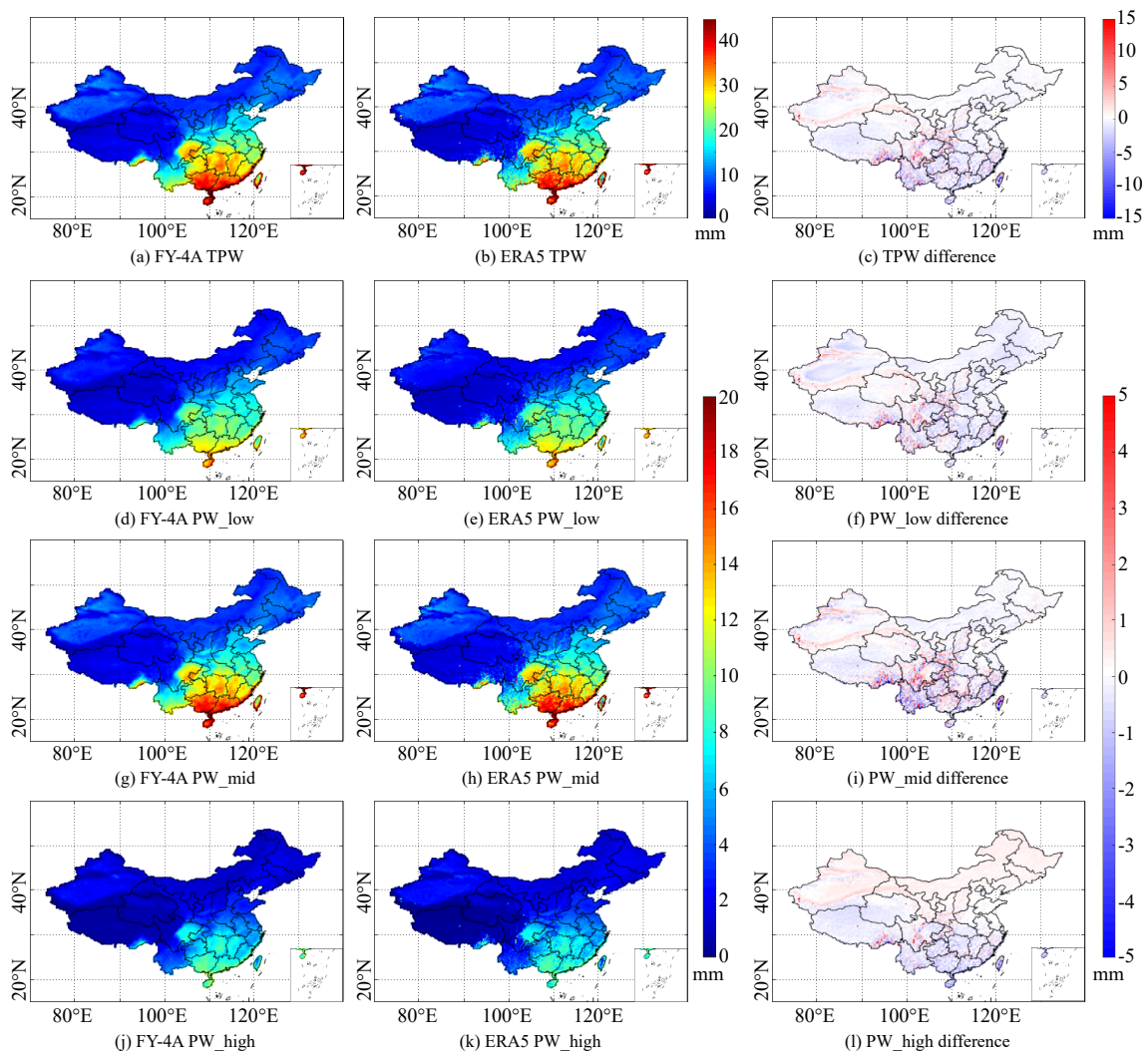


Figure 6. Spatial distribution of four LPW products from FY-4A and ERA5, along with the differences between the two observations (difference = ERA5–FY-4A).

4. Comparative Analysis of FY-4A LPWs Over Various Climatic Regions

As mentioned above, it is necessary to analyze the performance and variation characteristics of FY-4A LPW products in various climatic areas, which play an important role in studying the atmospheric water vapor variations and distributions with FY-4A water vapor products. In this section, we systematically analyze the performance of FY-4A LPW products over five climatic regions in China.

4.1. Temperate Monsoon Climatic Region

Figure 7a shows the seasonal variation in LPWs over the temperate monsoon climatic area, where the weather is humid, hot, and rainy in summer, with an FY-4A TPW of 28.24 mm and an ERA5 TPW of 27.44 mm. In winter, it is quite cold and dry, with the lowest FY-4A TPW value of 2.84 mm in December. The other three layer PW products (i.e., PW_low, PW_mid, and PW_high) display the similar seasonal trend that they reach peak value in July and valley value in December, respectively. Compared to the ERA5 dataset, it is noticeable that FY-4A observations overestimate the LPWs between May and October (FY-4A vs. ERA5: 21.06 mm vs. 20.42 mm in TPW, 7.67 mm vs. 7.37 mm in PW_low, 9.23 mm vs. 8.97 mm in PW_mid, 4.09 mm vs. 4.08 mm in PW_high).

Furthermore, it is evident that TPW and the other three LPWs show the consistent temporal and spatial variations for the same climatic region. Meanwhile, TPW, referring to the total water vapor content among the atmosphere, is a key factor in meteorological processes and atmospheric dynamics. Therefore, taking TPW as a representative, we analyze its spatial variations under the different seasons in Figure 7b–d, which illustrate the spatial distribution of mean, RMSE, and MB for FY-4A TPW products, respectively. The mean TPW value is about 30 mm in summer, which is seven times that in winter (4.25 mm). In spring (March to May) and autumn (September to November), there is little difference in water vapor content for the whole climatic region. As for RMSE and MB, both have similar seasonal patterns and spatial distribution characteristics. The mean RMSE of four seasons is 1.58, 3.30, 1.66, and 0.96 mm (spring, summer, autumn, and winter), respectively. In bias variations, FY-4A observations overestimate the TPW values in a large proportion of the climatic region for spring, summer, and autumn, with MB values of -0.13 , -0.80 , and -0.27 mm, while it evidently underestimates TPW in winter (with a value of 0.58 mm). Furthermore, the southwest of the climatic area, i.e., Qinling mountain, which is regarded as the line of demarcation between southern and northern China, exhibits RMSE and MB that are significantly higher than the other regions in all seasons, which reveals that mountains play an important influence on the distribution and retrieval of atmospheric water vapor.

The seasonal overall comparisons (Figure 7e) between FY-4A observations and ERA5 data indicate good agreement, with average R values of 0.98, 0.98, 0.97, and 0.95 for the four LPW products. For each LPW product, it is distinguished by different colors in different seasons. The red line in each subfigure represents the fitting performance of the whole year observations for each LPW data point. It can be observed that the RMSE value of all four LPWs is less than 2 mm, particularly lower than 1 mm for PW_low and PW_high, which demonstrates that the high spatiotemporal FY-4A LPW products can properly represent the atmospheric water vapor over the temperate monsoon climatic area.

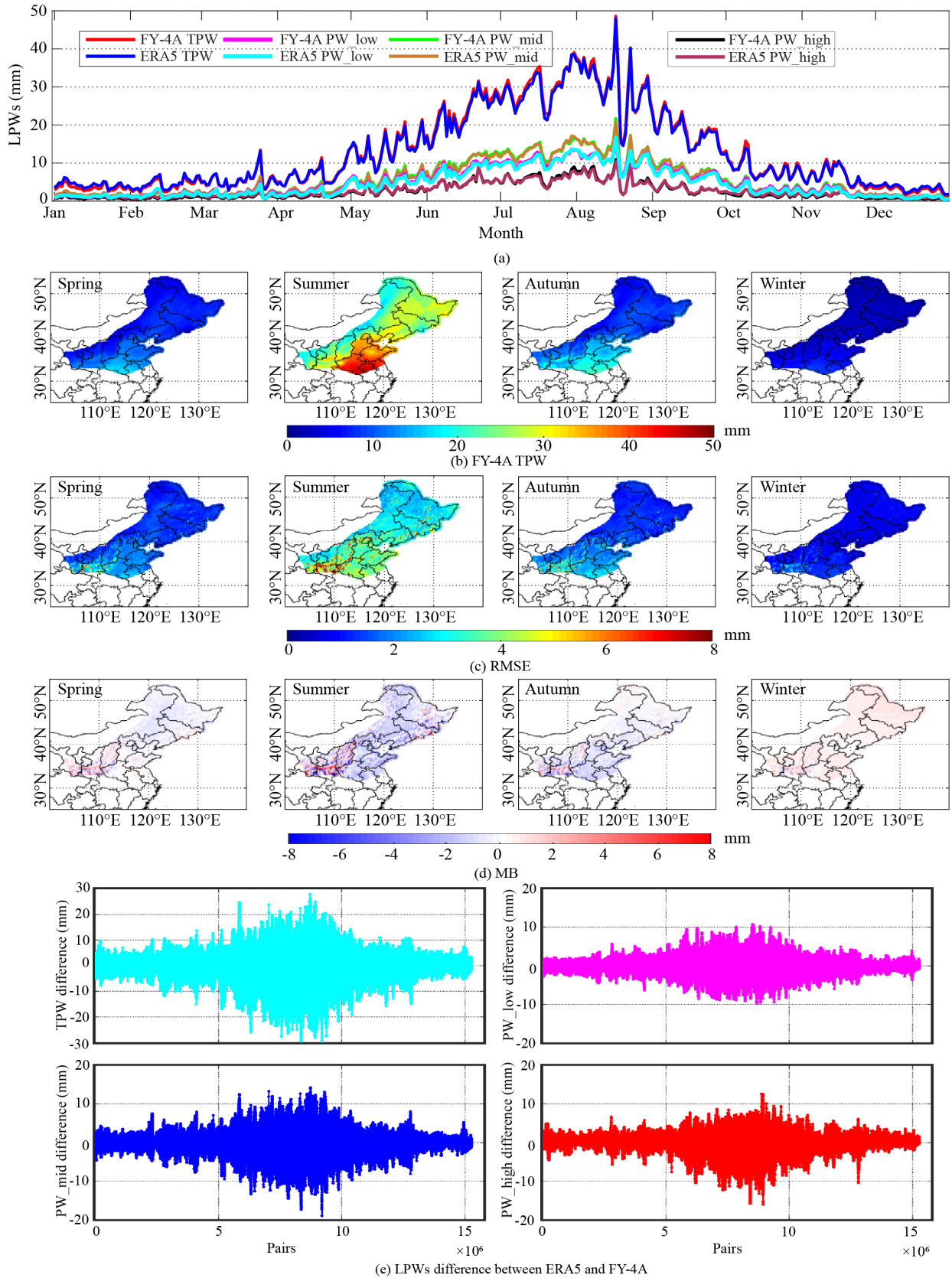


Figure 7. Spatial and seasonal variations of FY-4A LPW products and their accuracy in temperate monsoon region. (a) The daily mean of TPW values from FY-4A satellite observations and ERA data; (b–d) the spatial variation in mean, RMSE, and MB of FY-4A TPW over four seasons, respectively; (e) scatterplots of the ERA5 LPWs vs. FY-4A LPWs.

4.2. Temperate Continental Climatic Region

The temperate continental climatic region spans a large longitude range from 75 °E to 120 °E, with the Inner Mongolian Plateau, the Taklamakan Desert, and the Tarim Basin. Therefore, the area suffers from formidable natural conditions, resulting in a dry climate, low rainfall, and high evaporation [34]. The seasonal variations in LPWs are shown in Figure 8a, with a maximum FY-4A TPW of 18.59 mm in July and a minimum value of 2.86 mm in December. As for the other three LPW products, all observations fluctuate between 0 and 10 mm.

Figure 8b–d display a marked seasonal difference in mean, RMSE, and MB. The spatial distributions of TPW are consistent in spring and autumn, with a value about 7 mm, accounting for a third of the TPW value in summer, while TPW in winter only approximates 3.5 mm in most areas. Approximately 13 mm amplitude for FY-4A TPW from spring to summer and summer to autumn indicates the significant influence of less rainy and dry weather on the amount of water vapor. In view of the variations in RMSE, its peak value occurs in summer, with a value of 2.83 mm, and a minimum of 0.94 mm in winter. However, in the region bordering the plateau mountain climatic area, due to the dramatic variations in altitude, it is observed that the RMSE and MB of the contiguous area are larger than that of the rest of the climatic region.

Furthermore, as for the three typical topographical conditions (Inner Mongolian Plateau, Taklamakan Desert, and Tarim Basin) within this climatic area, in summer, due to the influence of high evaporation, the TPW values in the desert and basin are less than that in the Inner Mongolian Plateau. However, in spring and autumn, the first two regions show higher TPW contents. In addition, the plateau performs a slightly smaller RMSE value than the other two regions in the four seasons, and the MB is also characterized by a similar spatial distribution tendency. These comparisons imply the good retrieval performance of FY-4A observations in the Inner Mongolian Plateau.

In the comparison of FY-4A LPWs and ERA5 LPWs (Figure 8e), the MBs of the four FY-4A LPW products are 0.21 mm, −0.09 mm, 0.02 mm, and 0.31 mm, respectively, which indicates that PW_low is slightly overestimated by the AGRI instrument, and TPW and PW_high are underestimated, while FY-4A PW_mid observations agree well with the ERA5 data. The RMSE and R for the four LPWs are 1.80 mm/0.96, 0.71 mm/0.93, 0.93 mm/0.95, and 0.78 mm/0.90 separately. It can be found that although the RMSE of TPW is significantly greater than that of the other three products, it has the best correlation coefficient.

4.3. Plateau Mountain Climatic Region

The Qinghai–Tibet Plateau (QTP) is the main part of the plateau mountain climatic region, which is the birthplace of most of the rivers in Asia and is known as the “Asian water tower” [35]. Consequently, QTP plays a vital role in the regional climate change and global water cycle and thus has an important impact on human life and social development [36]. Figure 9a shows the day-to-day variation in LPWs over the plateau mountain climatic region. Evidently, due to the high altitude topography, the content of LPWs is low throughout the year, with an annual mean value of 5.05 mm, 1.85 mm, 2.32 mm, and 0.88 mm for the four FY-4A LPW products. As for the seasonal tendency, the FY-4A TPW peaks at a value of 10.99 mm in July and then drops to a minimum of 1.76 mm in December. The other three LPWs also display the same seasonal pattern.

For the spatial distribution of FY-4A products, Figure 9b illustrates that the mean of TPW is mainly located at 5 to 10 mm over QTP in summer, while in the other three seasons, the values are only about 3 mm. In the north of this climatic area, i.e., the Tianshan Mountain, FY-4A TPW is higher than that of QTP for all seasons. In view of the RMSE (Figure 9c) and MB (Figure 9d), the two statistics in summer (2.94 mm and −0.33 mm) imply more obvious errors in FY-4A TPW products than other seasons. This can be explained by the fact that the RMSE and MB of TPW mainly depend on the amount of water vapor products obtained from AGRI observations.

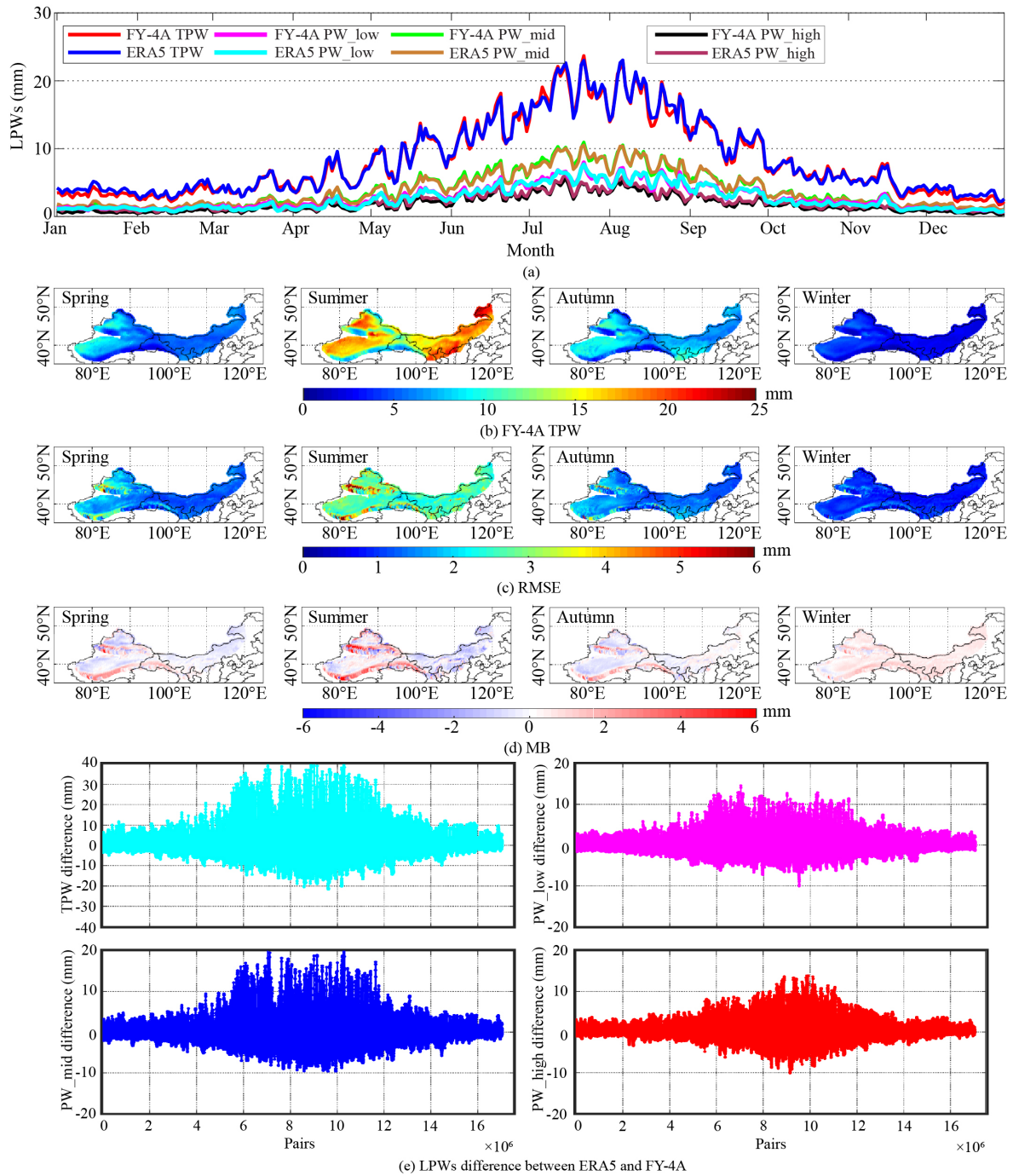


Figure 8. Spatial and seasonal variations in FY-4A LPW products and their accuracy in temperate continental region. (a) The daily mean of TPW values from FY-4A satellite observations and ERA data; (b–d) the spatial variation in mean, RMSE, and MB of FY-4A TPW over four seasons, respectively; (e) scatterplots of the ERA5 LPWs vs. FY-4A LPWs.

Furthermore, when comparing the FY-4A LPWs with the ERA5 data, it is noticeable from Figure 9e that the FY-4A TPW and PW_high products underestimate the water vapor values (the MB of -0.09 mm and -0.11 mm), while FY-4A PW_low and PW_mid observations show good agreement with the ERA5 data (0.03 and 0.01 mm in MB). The RMSE of the four LPW products are 2.26, 0.77, 1.04, and 0.86 mm, respectively. However, the correlation of all LPWs in the research area are not as good as that in the above two regions; the R only reaches about 0.86 for TPW, PW_low, and PW_mid, even 0.71 for PW_high. This may be due to the complex topography and atmospheric conditions,

which create significant spatial heterogeneity in moisture distribution. Additionally, the FY-4A LPW products may be more sensitive to terrain-induced factors, such as elevation changes, cloud cover, and surface reflectance, which can impact the accuracy of satellite-based observations.

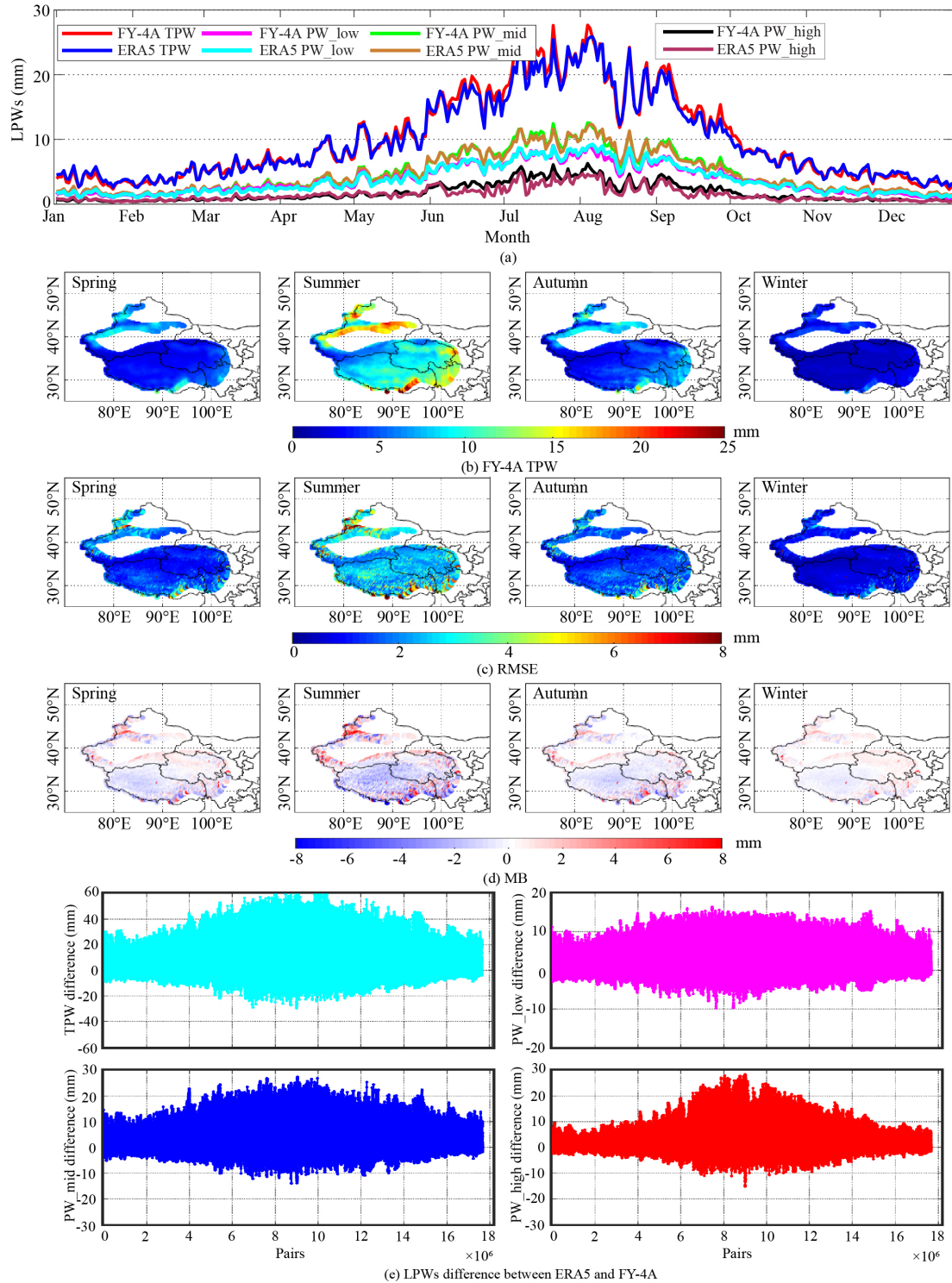


Figure 9. Spatial and seasonal variations in FY-4A LPW products and their accuracy in plateau mountain region. (a) The daily mean of TPW values from FY-4A satellite observations and ERA data; (b–d) the spatial variation in mean, RMSE, and MB of FY-4A TPW over four seasons, respectively; (e) scatterplots of the ERA5 LPWs vs. FY-4A LPWs.

4.4. Subtropical Monsoon Climatic Region

The subtropical monsoon climatic region covers the southeast and southwest regions of China, with the longitude from 92° to 122° and latitude from 21° to 34°. There are various rivers and lakes in the region, and therefore, it is rainy and humid. Figure 10a shows a marked seasonal cycle in the daily mean LPWs from January to December 2020. The maximum FY-4A TPW occurs in July, with a value of 46.11 mm, and the minimum value is 12.54 mm in December. The mean TPW in spring and autumn are roughly the same, with values of 23.26 mm and 30.14 mm. The spatial distribution of the FY-4A TPW value is displayed in Figure 10b. It is noticeable that the west of the climatic area always shows a smaller TPW value than the other region in the four seasons. As for the other regions, the TPW product exceeds 50 mm in summer, while in winter, it fluctuates between 10 mm and 20 mm. In spring and autumn, its value is about 20 mm higher than that in winter.

Figure 10c,d demonstrate the accuracy changes in FY-4A TPW in different seasons, with mean RMSE and MB of 3.73/−0.44 mm, 5.06/−0.39 mm, 3.66/−1.23 mm, and 2.29/−0.07 mm in the four seasons, respectively. Similar results have been observed that the accuracy is better in the winter than in the spring and autumn, and it is worst in the summer. As discussed above, this is because of the obvious dependence of RMSE and MB on the amount of water vapor. Furthermore, the geographical distributions of the statistics have found that the RMSE and MB gradually decline from west to east of the study area. This is because the altitude of the research area is decreased from plateau (west) to plain (east), contributing to the remission of the influence of topography. For the overall comparisons of the four LPW products (Figure 10e), the RMSE of TPW and PW_mid are 4.23 mm and 2.14 mm compared to the ERA5 data, respectively, which are higher than that of PW_low (1.37 mm) and PW_high (1.64 mm). In addition, all four FY-4A LPWs overestimate the water vapor contents in this climatic region, with MB values of −0.51, −0.13, −0.06, and −0.23 mm, respectively. Furthermore, the R of all LPWs is greater than 0.94, indicating a good agreement between the two observations.

4.5. Tropical Monsoon Climatic Region

Figure 11a illustrates the LPW cycle in the tropical monsoon climatic region, in which the monthly mean value of FY-4A TPW in most months is larger than 25 mm, revealing the large water vapor contents in the research area. In addition, the seasonal mean TPW is 34.96, 49.36, 39.23, and 22.00 mm for four seasons (spring, summer, autumn, and winter), respectively, which does not show the same remarkable seasonal trend as in the above climatic areas. It peaks in June with a value of 49.63 mm and reaches the lowest value of 20 mm in February. For the PW_low, PW_mid, and PW_high products, most of them vary between 5 mm and 20 mm in the whole year of 2020. Figure 11b displays the spatial distribution of TPW in tropical monsoon climatic area, which includes three regions: the southernmost part of Yunnan, the Hainan Island, and the south of Taiwan. It is evident that in the four seasons, the TPW value of the Hainan Island is the highest, followed by the south of Taiwan, and the southernmost part of Yunnan shows the minimum value. In terms of the seasonal variations, the small TPW changes can be seen in the climatic area from spring to autumn, whereas the TPW contents dramatically decrease in the winter.

For the assessment of FY-4A TPW products (Figure 11c,d), the RMSE and MB do not show obvious variations for different seasons (with the two statistics of 5.34/−1.96 mm, 5.60/−1.44 mm, 4.87/−1.41 mm, and 4.04/−1.16 mm in the four seasons). Meanwhile, for the three main regions within the climatic area, the RMSE and MB of these regions are not much different. Figure 11e indicates that the four FY-4A LPW products agree well with the ERA5 data. The RMSE of TPW is 5.33 mm, ranked first among the four LPWs. The RMSE of the other three LPWs are 1.76, 2.73, and 2.01 mm, respectively. Additionally, similar to the subtropical monsoon climatic region, all four LPW products are overestimated with the AGRI sensors, with the MB of −1.41, −0.07, −0.50, and −0.72 mm.

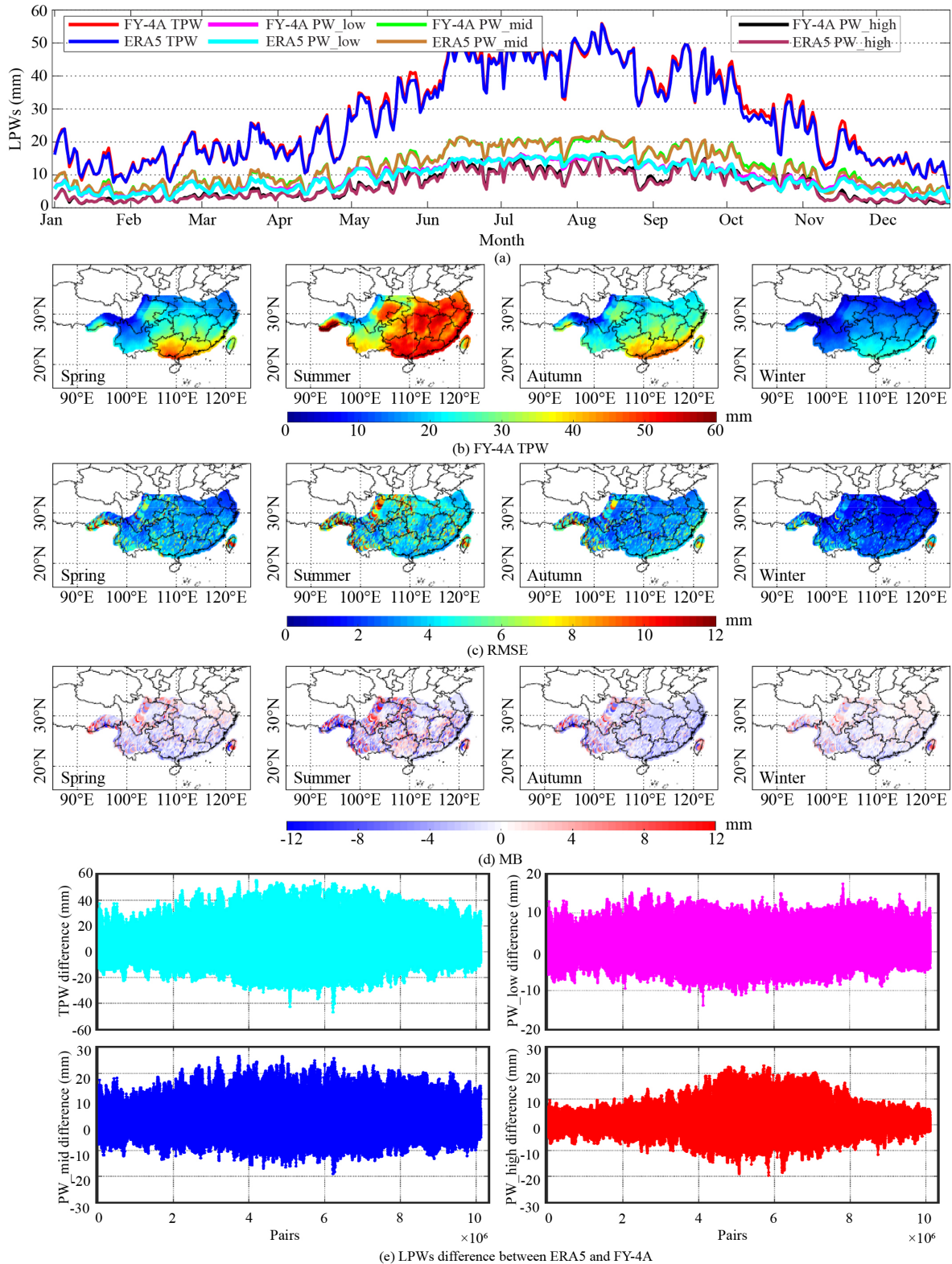


Figure 10. Spatial and seasonal variations in FY-4A LPW products and their accuracy in subtropical monsoon region. (a) The daily mean of TPW values from FY-4A satellite observations and ERA data; (b–d) the spatial variation in mean, RMSE, and MB of FY-4A TPW over four seasons, respectively; (e) scatterplots of the ERA5 LPWs vs. FY-4A LPWs.

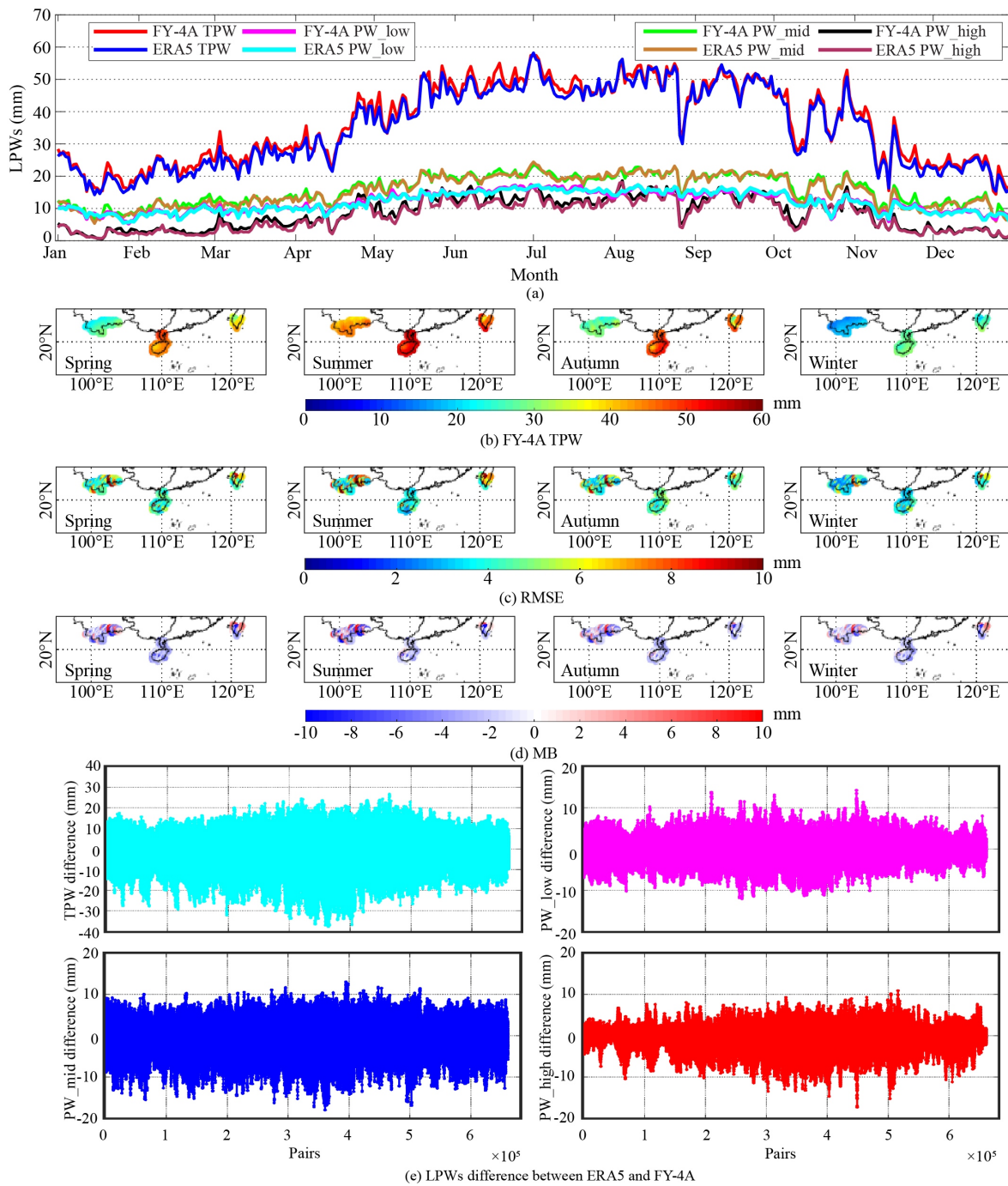


Figure 11. Spatial and seasonal variations in FY-4A LPW products and their accuracy in tropical monsoon region. (a) The daily mean of TPW values from FY-4A satellite observations and ERA5 data; (b–d) the spatial variation in mean, RMSE, and MB of FY-4A TPW over four seasons, respectively; (e) scatterplots of the ERA5 LPWs vs. FY-4A LPWs.

5. Discussion

As shown in Section 4, the performance of the four FY-4A LPW products in five typical climatic areas are analyzed by comparing LPW retrievals from the hourly ERA5 data. It can be observed that all LPW observations display a considerable accuracy on the millimeter level. However, owing to the changes in climate zones and seasonal patterns, FY-4A observations show the variable accuracy and stability in different cases. Therefore, we compare the performance of FY-4A LPW products in different climatic regions and seasons.

5.1. Cross Comparison of Five Climate Zones

The five climatic regions in China show distinct climate and topographical characteristics, which lead to significant spatial heterogeneity for LPW products. In the study by Bai et al. [25], they evaluated MODIS PWV products using GPS PWV data over the five climate regions in China and found that MODIS overestimates PWV in a temperate continental climatic region while underestimating water vapor in other climate regions.

In this section, Table 1 lists the statistics (mean, RMS, MB) of FY-4A TPW products as it includes the variation characteristics of the other three sets of LPW data. It is noticeable that because of the effect of tropical revolving storms, the TPW value in the tropical monsoon area is significantly higher than those in the other four climatic regions during all seasons (mean TPWs of 12.41, 8.24, 5.10, 26.58, and 34.64 mm in the five areas), and thus, the RMS and MB also peaked in this region, with averages of 4.96 mm and -1.49 mm, respectively. On the contrary, the plateau mountain region generates a minimum TPW value of 5.10 mm due to the high altitude, while its RMS is not the lowest, with a value of 1.77 mm, which is slightly larger than the RMS in the temperate continental area (1.72 mm). The TPW value in the subtropical monsoon area is 26.58 mm, ranking second among the five zones. Similarly, the statistics in this region have the same ranking (RMSE = 3.69 mm, MB = -0.53 mm). As for the temperate monsoon and temperate continental regions, they yield close water vapor contents and accuracy, with TPW = 12.41 mm and RMS = 1.88 mm in the former and TPW = 8.24 mm and RMS = 1.72 mm in the latter.

It can be concluded from the above comparisons that FY-4A LPWs are underestimated in the temperate monsoon area and overestimated in the subtropical and tropical monsoon regions, while FY-4A measurement agrees well with ERA5 reanalysis in temperate continental and plateau mountain zones.

Table 1. Mean, RMS, and MB of the difference between ERA5 and FY-4A TPW products over the five regions and four seasons (unit: mm).

Climatic Area	Season	Spring	Summer	Autumn	Winter	Overall
Temperate monsoon	Mean	8.27	27.36	10.44	3.56	12.41
	RMS	1.58	3.30	1.66	0.96	1.88
	MB	-0.13	-0.80	-0.27	0.58	-0.16
Temperate continental	Mean	6.23	16.06	7.44	3.23	8.24
	RMS	1.58	2.83	1.53	0.94	1.72
	MB	-0.01	0.18	0.01	0.52	0.18
Plateau mountain	Mean	3.87	9.91	4.76	1.85	5.10
	RMS	1.57	2.94	1.72	0.85	1.77
	MB	-0.07	-0.33	-0.12	0.16	-0.09
Subtropical monsoon	Mean	23.44	43.20	26.01	13.67	26.58
	RMS	3.73	5.06	3.66	2.29	3.69
	MB	-0.44	-0.39	-1.23	-0.07	-0.53
Tropical monsoon	Mean	33.69	46.44	36.46	21.98	34.64
	RMS	5.34	5.60	4.87	4.04	4.96
	MB	-1.96	-1.44	-1.41	-1.16	-1.49
Overall	Mean	15.10	28.59	17.02	8.86	17.39
	RMS	2.76	3.95	2.69	1.82	2.80
	MB	-0.52	-0.56	-0.60	0.01	-0.42

5.2. Seasonal Variations

In terms of the FY-4A TPW products during the four seasons, it is evident that the TPW in all five regions reached the largest values in summer (27.36, 16.06, 9.91, 43.20, and 46.44 mm) and smallest values in winter (3.56, 3.23, 1.85, 13.67, and 21.98 mm). In spring and autumn, both temperate continental and plateau mountain regions show close TPW observations and RMS values, while in the other three areas, an amplification of about

2.5 mm from spring to autumn can be found in the TPW value. Meanwhile, the statistics perform consistent seasonal variation characteristics with TPW products. As for the whole China region, the TPW and RMS values in summer are 28.59 mm and 3.95 mm, which are three times the TPW and twice the RMS in winter, respectively (TPW = 8.86 mm and RMS = 1.82 mm). In spring and autumn, the PWV values are 15.10 mm and 17.02 mm, accounting for nearly half of the TPW in summer. In summary, the atmospheric water vapor distributions are affected by a lot of factors, such as climate, season, and terrain, which lead to the significant variations and differences over China.

6. Conclusions

In this paper, in view of the significant climatic and seasonal changes in China, we evaluate and analyze the climatic and seasonal variations in FY-4A LPW products over five climatic regions, which is significant for understanding the reliability and variability of FY-4A LPW water vapor retrievals. We used the four hourly LPW products (TPW, PW_low, PW_mid, and PW_high) with the resolution of 0.25° obtained from the latest ERA5 atmospheric reanalysis as a reference. Moreover, to match the stratification of FY-4A LPW products, we proposed a surface pressure calibration algorithm for ERA5 LPW products based on DEM data. The overall validations of the latest FY-4A LPW observations show that all four FY-4A LPW products generally agree with the ERA5 LPWs, with the RMSE and MB of 2.58/−0.08, 0.90/−0.09, 1.30/−0.02, and 1.01/0.11 mm for the four LPW products, respectively. Furthermore, the deep analyses between FY-4A LPW products and ERA5 data from the perspectives of the climate dependencies and seasonal patterns have been performed. The main results are concluded below:

1. The accuracy of the four FY-4A LPW products changes significantly throughout the five climatic regions in China. RMSE peaks at a value of 2.96 mm in the tropical monsoon area and reaches a minimum of 1.06 mm in the temperate continental zone. Furthermore, the FY-4A LPW products are overestimated in subtropical and tropical monsoon zones, with MB values of −0.23 and −0.68 mm, respectively, and underestimated in the temperate monsoon region (MB = 0.14 mm). In the other two regions, FY-4A LPWs show a good agreement with the ERA5 data.
2. The four LPWs are characterized by the same seasonal tendency that LPW products gradually increase from spring to the beginning of summer and dramatically reach the peak in the medium of summer and then decrease continuously until winter. Taking TPW products as an example, they have the highest value of 3.95 mm in summer, which is 1.5 times that in spring and autumn (2.76 and 2.69 mm) and twice that in winter (1.82 mm). Among the five climatic regions, the RMSE and MB of FY-4A TPW observations illustrate similar seasonal patterns in the first four regions, while in the tropical monsoon area, the RMSE fluctuates between 4 mm and 5.6 mm during all seasons.
3. When FY-4A LPW products are applied to water vapor studies over China, the variations in difference in different climatic areas and seasons should be considered, and a climate- and season-related calibration model is essential for enhancing the performance of FY-4A water vapor products. This has a significant influence on the climate change and other meteorological studies in China.

Author Contributions: Conceptualization, W.Z. and X.X.; methodology, W.Z.; software, J.P.; validation, X.X. and J.P.; formal analysis, E.S.; investigation, G.M.; resources, X.X.; data curation, J.P.; writing—original draft preparation, W.Z.; writing—review and editing, G.M.; visualization, W.Z.; supervision, S.Z.; project administration, W.Z.; funding acquisition, S.Z. All authors have read and agreed to the published version of the manuscript.

Funding: This research was funded by the National Natural Science Foundation of China, grant number 42404016 and 42271460, by the Natural Science Foundation of Jiangsu Province, grant number BK20241669, by the Fundamental Research Funds for the Central Universities, grant number

2024QN11077, by the Advantaged Discipline Construction Project of University in Jiangsu Province (Surveying and Mapping Science and Technology Discipline).

Institutional Review Board Statement: Not applicable.

Informed Consent Statement: Not applicable.

Data Availability Statement: The data presented in this study are available on request from the corresponding author because the data are part of an ongoing study.

Acknowledgments: The authors acknowledge the support of ECMWF for providing the ERA5 products and Fengyun Satellite Data Center for the provision of FY-4A LPW data. The anonymous reviewers and editor are acknowledged for their meaningful reviews and suggestions.

Conflicts of Interest: The authors declare no conflicts of interest.

Abbreviations

The following abbreviations are used in this manuscript:

LPW	Layer precipitable water
PWV	Precipitable water vapor
TPW	Total perceptible water
PW_low	Low layer perceptible water
PW_mid	Middle layer perceptible water
PW_high	High layer perceptible water
FY-4A	Fengyun-4A
AGRI	Advanced Geosynchronous Radiation Imager
ECMWF	European Centre for Medium-Range Weather Forecasts
ERA5	Fifth generation ECMWF atmospheric reanalysis
DEM	Digital elevation model
RMSE	Root mean square error
MB	Mean bias
R	Correlation coefficient
IDW	Inverse distance weighted
QTP	Qinghai–Tibet Plateau

References

1. Sherwood, S.C.; Roca, R.; Weckwerth, T.M.; Andronova, N.G. Tropospheric water vapor, convection, and climate. *Rev. Geophys.* **2010**, *48*, 1–29. [[CrossRef](#)]
2. Shi, J.; Xu, C.; Guo, J.; Gao, Y. Real-Time GPS Precise Point Positioning-Based Precipitable Water Vapor Estimation for Rainfall Monitoring and Forecasting. *IEEE Trans. Geosci. Remote Sens.* **2015**, *53*, 3452–3459.
3. Wang, X.; Zhang, K.; Wu, S.; Li, Z.; Cheng, Y.; Li, L.; Yuan, H. The correlation between GNSS-derived precipitable water vapor and sea surface temperature and its responses to El Niño–Southern Oscillation. *Remote Sens. Environ.* **2018**, *216*, 1–12. [[CrossRef](#)]
4. Chen, Z.; Li, L.; Wang, B.; Fan, J.; Lu, T.; Lv, K. The impact of global warming on ENSO from the perspective of objective signals. *Atmos. Res.* **2023**, *299*, 107176. [[CrossRef](#)]
5. Li, J.; Yang, F.; Yuan, D.; Wang, H.; Song, S.; Tan, J.; Wen, Z. Unraveling the Accuracy Enigma: Investigating ZTD Data Precision in TUW-VMF3 and GFZ-VMF3 Products Using a Comprehensive Global GPS Dataset. *IEEE Trans. Geosci. Remote Sens.* **2024**, *62*, 1–10. [[CrossRef](#)]
6. Bevis, M.; Businger, S.; Herring, T.A.; Rocken, C.; Anthes, R.A.; Ware, R.H. GPS meteorology: Remote sensing of atmospheric water vapor using the global positioning system. *J. Geophys. Res. Atmos.* **1992**, *97*, 15787–15801. [[CrossRef](#)]
7. Yang, F.; Sun, Y.; Meng, X.; Guo, J.; Gong, X. Assessment of tomographic window and sampling rate effects on GNSS water vapor tomography. *Satell. Navig.* **2023**, *4*, 7. [[CrossRef](#)]
8. Ichoku, C.; Levy, R.; Kaufman, Y.J.; Remer, L.A.; Li, R.R.; Martins, V.J.; Holben, B.N.; Abuhassan, N.; Slutsker, I.; Eck, T.F.; et al. Analysis of the performance characteristics of the five-channel Microtops II Sun photometer for measuring aerosol optical thickness and precipitable water vapor. *J. Geophys. Res. Atmos.* **2002**, *107*, AAC–5. [[CrossRef](#)]
9. Leontiev, A.; Rostkier-Edelstein, D.; Reuveni, Y. On the potential of improving WRF model forecasts by assimilation of high-resolution GPS-derived water-vapor maps augmented with METEOSAT-11 data. *Remote Sens.* **2020**, *13*, 96. [[CrossRef](#)]
10. Zhang, W.; Zhang, S.; Ding, N.; Holden, L.; Wang, X.; Zheng, N. GNSS-RS Tomography: Retrieval of Tropospheric Water Vapor Fields Using GNSS and RS Observations. *IEEE Trans. Geosci. Remote Sens.* **2022**, *60*, 1–13. [[CrossRef](#)]
11. Zhao, Q.; Liu, Y.; Ma, X.; Yao, W.; Yao, Y.; Li, X. An improved rainfall forecasting model based on GNSS observations. *IEEE Trans. Geosci. Remote Sens.* **2020**, *58*, 4891–4900. [[CrossRef](#)]

12. Saha, J.; Price, C.; Plotnik, T.; Guha, A. Impact of the El Niño–Southern Oscillation on upper-tropospheric water vapor. *Atmos. Res.* **2022**, *280*, 106422. [[CrossRef](#)]
13. Schmit, T.J.; Li, J.; Lee, S.J.; Li, Z.; Dworak, R.; Lee, Y.K.; Bowlan, M.; Gerth, J.; Martin, G.D.; Straka, W.; et al. Legacy Atmospheric Profiles and Derived Products From GOES-16: Validation and Applications. *Earth Space Sci.* **2019**, *6*, 1730–1748. [[CrossRef](#)]
14. Wang, P.; Li, J.; Lu, B.; Schmit, T.J.; Lu, J.; Lee, Y.K.; Li, J.; Liu, Z. Impact of Moisture Information From Advanced Himawari Imager Measurements on Heavy Precipitation Forecasts in a Regional NWP Model. *J. Geophys. Res. Atmos.* **2018**, *123*, 6022–6038. [[CrossRef](#)]
15. Pan, S.; Gao, J.; Jones, T.A.; Wang, Y.; Li, J. The Impact of Assimilating Satellite-Derived Layered Precipitable Water, Cloud Water Path, and Radar Data on Short-Range Thunderstorm Forecasts. *Mon. Weather Rev.* **2021**, *149*, 1359–1380. [[CrossRef](#)]
16. Wang, Y.; Liu, H.; Zhang, Y.; Duan, M.; Tang, S.; Deng, X. Validation of FY-4A AGRI layer precipitable water products using radiosonde data. *Atmos. Res.* **2021**, *253*, 105502. [[CrossRef](#)]
17. Zhang, Y.; Li, Z.; Li, J. A Preliminary Layer Perceptible Water Vapor Retrieval Algorithm for Fengyun-4 Advanced Geosynchronous Radiation Imager. In Proceedings of the IGARSS 2019—2019 IEEE International Geoscience and Remote Sensing Symposium, Yokohama, Japan, 28 July–2 August 2019; pp. 7564–7566.
18. Zhai, P.; Eskridge, R.E. Atmospheric water vapor over China. *J. Clim.* **1997**, *10*, 2643–2652. [[CrossRef](#)]
19. Yuan, P.; Hunegnaw, A.; Alshawaf, F.; Awange, J.; Klos, A.; Teferle, F.N.; Kutterer, H. Feasibility of ERA5 integrated water vapor trends for climate change analysis in continental Europe: An evaluation with GPS (1994–2019) by considering statistical significance. *Remote Sens. Environ.* **2021**, *260*, 112416. [[CrossRef](#)]
20. Zhang, P.; Zhu, L.; Tang, S.; Gao, L.; Chen, L.; Zheng, W.; Han, X.; Chen, J.; Shao, J. General comparison of FY-4A/AGRI with other GEO/LEO instruments and its potential and challenges in non-meteorological applications. *Front. Earth Sci.* **2019**, *6*, 224. [[CrossRef](#)]
21. Zhang, J.; Zhiguang, L. *Climate of China*; John Wiley & Sons: Hoboken, NJ, USA, 1992.
22. Gao, X.; Shi, Y.; Zhang, D.; Giorgi, F. Climate change in China in the 21st century as simulated by a high resolution regional climate model. *Chin. Sci. Bull.* **2012**, *57*, 1188–1195.
23. Zhang, X.; Yan, X. Temporal change of climate zones in China in the context of climate warming. *Theor. Appl. Climatol.* **2014**, *115*, 167–175. [[CrossRef](#)]
24. Administration, C.M. *Atlas of Climate of the P.R. of China*; SinoMaps Press: Beijing, China, 1979.
25. Bai, J.; Lou, Y.; Zhang, W.; Zhou, Y.; Zhang, Z.; Shi, C. Assessment and calibration of MODIS precipitable water vapor products based on GPS network over China. *Atmos. Res.* **2021**, *254*, 105504. [[CrossRef](#)]
26. Hersbach, H.; Bell, B.; Berrisford, P.; Hirahara, S.; Horányi, A.; Muñoz-Sabater, J.; Nicolas, J.; Peubey, C.; Radu, R.; Schepers, D.; et al. The ERA5 global reanalysis. *Q. J. R. Meteorol. Soc.* **2020**, *146*, 1999–2049. [[CrossRef](#)]
27. Zhang, W.; Zhang, H.; Liang, H.; Lou, Y.; Cai, Y.; Cao, Y.; Zhou, Y.; Liu, W. On the suitability of ERA5 in hourly GPS precipitable water vapor retrieval over China. *J. Geod.* **2019**, *93*, 1897–1909. [[CrossRef](#)]
28. Yang, J.; Zhang, Z.; Wei, C.; Lu, F.; Guo, Q. Introducing the new generation of Chinese geostationary weather satellites, Fengyun-4. *Bull. Am. Meteorol. Soc.* **2017**, *98*, 1637–1658. [[CrossRef](#)]
29. Wessel, B. *TanDEM-X Ground Segment—DEM Products Specification Document*; German Aerospace Center: Oberpfaffenhofen, Germany, 2018.
30. Hobiger, T.; Ichikawa, R.; Koyama, Y.; Kondo, T. Fast and accurate ray-tracing algorithms for real-time space geodetic applications using numerical weather models. *J. Geophys. Res. Atmos.* **2008**, *113*. [[CrossRef](#)]
31. Zhang, W.; Zhang, S.; Chang, G.; Ding, N.; Wang, X. A new hybrid observation GNSS tomography method combining the real and virtual inverted signals. *J. Geod.* **2021**, *95*, 1–18. [[CrossRef](#)]
32. Möller, G. Reconstruction of 3D Wet Refractivity Fields in the Lower Atmosphere Along Bended GNSS Signal Paths. Ph.D. Thesis, Technische Universität Wien, Vienna, Austria, 2017.
33. Chang, L.; Xiao, R.; Prasad, A.A.; Gao, G.; Feng, G.; Zhang, Y. Cloud mask-related differential linear adjustment model for MODIS infrared water vapor product. *Remote Sens. Environ.* **2019**, *221*, 650–664. [[CrossRef](#)]
34. Zhang, X.; Li, X.; Zhang, H. The control of drift sand on the southern fringe of the Taklamakan Desert—An example from the Cele oasis. In *Sustainable Land Use in Deserts*; Springer: Berlin/Heidelberg, Germany, 2001; pp. 350–356.
35. Immerzeel, W.W.; Van Beek, L.P.; Bierkens, M.F. Climate change will affect the Asian water towers. *Science* **2010**, *328*, 1382–1385. [[CrossRef](#)]
36. Pritchard, H.D. Asia’s shrinking glaciers protect large populations from drought stress. *Nature* **2019**, *569*, 649–654. [[CrossRef](#)] [[PubMed](#)]

Disclaimer/Publisher’s Note: The statements, opinions and data contained in all publications are solely those of the individual author(s) and contributor(s) and not of MDPI and/or the editor(s). MDPI and/or the editor(s) disclaim responsibility for any injury to people or property resulting from any ideas, methods, instructions or products referred to in the content.